PAPER

Check for updates

A double probe-based fluorescence sensor array to detect rare earth element ions†

Hamada A. A. Noreldeen,‡[a,b] Chen-Ting Zhu,‡[a] Kai-Yuan Huang,[a] Hua-Ping Peng,[a] Hao-Hua Deng 🔟 *[a] and Wei Chen 🔟 *[a]

There is a persistent need for effective sensors to detect rare earth element ions (REEIs) due to their effects on human health and the environment. Thus, a simple and efficient fluorescence-based detection method for REEIs that offers convenience, flexibility, versatility, and efficiency is essential for ensuring environmental safety, food quality, and biomedical applications. In this study, 6-aza-2-thiothymine-gold nanoclusters (ATT-AuNCs) and bovine serum albumin/3-mercaptopropionic acid-AuNCs (BSA/MPA-AuNCs) were utilized to detect 14 REEIs (Sc^{3+}, Gd^{3+}, Lu^{3+}, Y^{3+}, Ce^{3+}, Pr^{3+}, Yb^{3+}, Dy^{3+}, Tm^{3+}, Sm^{3+}, Ho^{3+}, Tb^{3+}, La^{3+}, and Eu^{3+}), resulting in the creation of a simple, sensitive, and multi-target fluorescence sensor array detection platform. We observed that REEIs exert various enhancement or quenching effects on ATT-AuNCs and BSA/MPA-AuNCs. Thus, these two probes function as double signal channels, with the different effects of REEIs serving as signal inputs. Pattern recognition methods, including hierarchical cluster analysis (HCA) and linear discriminant analysis (LDA), were used to assess the recognition performance of the constructed sensing system. Beyond the excellent ability to recognize individual REEIs, the platform is also capable of distinguishing mixed REEIs. Also, this approach was validated by applying it to detect REEIs in purified water samples. This method not only minimizes the need for synthesizing and optimizing new probes but also offers a novel approach for the determination and identification of diverse analytes, filling a gap in the detection of a large number of REEIs simultaneously.

Introduction

Rare earth elements (REEs) are widely used across various fields due to their unique physical and chemical properties.[1–3] Naturally occurring in the human body, REE ion (REEI) concentrations are approximately 1 ng kg^{-1},[4] which is 1000 times lower than the LD_{50} (lethal dose for 50% of the population) of 1 mg kg^{-1} observed in mice.[5,6] Although REEIs have been shown to exhibit toxic effects on various organisms,[7] recent research has leveraged these toxic properties for cancer treatment.[8] For instance, some studies utilize the propensity of REEIs to compete with Ca^{2+} ions, reducing protein phosphorylation activity in astrocytes and thereby interrupting normal functions, leading to cell death.[9–12] With ongoing research, the applications of REEIs in biomedicine are expanding, such as cell labeling and imaging through REEI doping[13,14] and drug delivery using REEI-based metal–organic frameworks.[15–17] Thus, accurately detecting REEI concentrations is vital for both medical treatments and daily health monitoring. Current methods for detecting REEIs include atomic absorption spectroscopy (AAS), X-ray fluorescence spectroscopy (XFR), inductively coupled plasma atomic emission spectroscopy (ICP-AES), and inductively coupled plasma mass spectrometry (ICP-MS).[18–21] However, these technologies are time-consuming and require expensive equipment and complex procedures. Recently, fluorescence-based detection methods have gained attention due to their high sensitivity, simplicity, rapidity, and cost-effectiveness in detecting REEIs.[22–24] Therefore, using an easy and simple fluorescence-based detection approach for REEIs could provide a convenient, versatile, efficient, and valuable tool for ensuring environmental safety and food quality.

The fluorescence sensor array is a novel method developed from fluorescence analysis.[25] Compared to traditional detection methods, the fluorescence sensor array not only retains the advantages of conventional fluorescence analysis but also allows simultaneous detection and differentiation of multiple targets.[26–30] Much like the human taste system, the fluorescence sensing array consists of multiple sensing elements that exhibit cross-responses, generating a unique composite

[a]Fujian Key Laboratory of Drug Target Discovery and Structural and Functional Research, School of Pharmacy, Fujian Medical University, Fuzhou 350004, China. E-mail: DHH8908@163.com, chenandhu@163.com; Fax: +86 591 22862016; Tel: +86 591 22862016

[b]National Institute of Oceanography and Fisheries, NIOF, Cairo, Egypt

†Electronic supplementary information (ESI) available. See DOI: https://doi.org/10.1039/d4an01520g

‡These authors contributed equally to this work.

response for each analyte. This method relies on collecting multiple responses for each target, aiding in their identification. One of the key advantages of this approach is its reliance on analyzing various response patterns rather than specific receptor–target interactions.[27–29] Typically, the sensor array requires at least two analytical signals to detect multiple targets.[31–34] The target analytes have different effects on the probes, generating distinct signals for differential analysis.[31,35] Using linear discriminant analysis (LDA) and hierarchical cluster analysis (HCA) to analyze and process these signals, multidimensional data models are established to identify and determine unknown analytes. This approach overcomes the limitations of single-sensor, single-analyte detection, enabling high-throughput analysis.[36] Therefore, there is a great need for this technology to simultaneously detect the largest possible number of REEIs.

Gold nanoclusters (AuNCs), with diameters smaller than 2 nm, possess unique physical and chemical properties.[37–39] As a novel fluorescent material, AuNCs are characterized by easy preparation, functionalization, low toxicity, ultrafine particle size, good photostability, large Stokes shift, and tunable emission.[40–44] Additionally, due to the exceptional photoelectrochemical properties of AuNCs, they are extensively utilized in catalysis, ion and biomolecular monitoring and analysis, biological imaging, biomarkers, and various other fields.[29] These attributes make AuNCs ideal materials for sensing applications. While AuNCs have numerous applications, traditional detection methods typically employ a single probe to identify a single compound, following a lock-and-key approach.[28] This conventional method is limited in its ability to detect a variety of compounds with similar structures. However, recent advancements have seen the use of AuNCs in developing sensor arrays for broader applications, including detecting heavy metal ions,[45–48] proteins,[49–51] small molecules,[52–55] bacteria,[55] and cells.[56] However, research on the application of sensor arrays to detect REEIs using AuNCs is limited, particularly for the detection of multiple REEIs. Therefore, a method that addresses the significant gap in using AuNC-based sensor arrays for detecting REEIs, combining the advantages of AuNCs and sensor array technology and offering stable output signals, simple operation, and sensitive detection, is essential for effective REEI detection.

Our previous research demonstrated that certain REEIs can affect the fluorescence of AuNCs. Specifically, it was found that Eu^{3+} significantly quenches the emission of AuNCs through a photoinduced electron transfer (PET) mechanism, while Sc^{3+} enhances the photoluminescence of AuNCs *via* the restriction of intramolecular motion (RIM) strategy.[57,58] Building on this concept, the present study employed two AuNC-based probes, namely 6-aza-2-thiothymine-gold nanoclusters (ATT-AuNCs) and bovine serum albumin/3-mercaptopropionic acid-AuNCs (BSA/MPA-AuNCs), to develop a fluorescence sensor array platform for detecting 14 REEIs (Sc^{3+}, Gd^{3+}, Lu^{3+}, Y^{3+}, Ce^{3+}, Pr^{3+}, Yb^{3+}, Dy^{3+}, Tm^{3+}, Sm^{3+}, Ho^{3+}, Tb^{3+}, La^{3+}, and Eu^{3+}). The results showed that this approach achieved a discrimination accuracy of 100%. This method was also applied to real samples (com-

mercially available purified water), maintaining 100% accuracy and demonstrating the platform's potential for comprehensive REEI detection. This is the first application of the AuNC-based fluorescence sensor array technology for the detection of a large number of REEIs, providing a basis for future applications of sensor arrays for on-site detection and other applications in different domains. The procedures of our sensing array for differentiating various REEIs are illustrated in Scheme 1.

Experimental section

Preparation of ATT-AuNCs

0.12 g of sodium hydroxide (NaOH) was dissolved in 15 mL of deionized water. Next, 0.17 g of 6-aza-2-thiothymine (ATT) powder was added to the prepared 0.20 mol L^{-1} NaOH solution. Then, 15 mL of $HAuCl_4$ (10 mg mL^{-1}) was added and mixed well. The mixture was stirred in a dark room at 30 °C for 2.5 hours. The resulting solution was purified by dialyzing it in deionized water using a 3500 KD dialysis bag for 24 hours. The purified solution was collected and stored at 4 °C under dark conditions.[59,60]

Preparation of BSA/MPA-AuNCs

0.625 g of bovine serum albumin (BSA) and 0.849 g of 3-mercaptopropionic acid (MPA) were dissolved in deionized water to prepare solutions with concentrations of 50 mg mL^{-1} and 4 mol L^{-1}, respectively. 12.5 mL of the BSA solution was mixed with 12.5 mL of $HAuCl_4$ (10 mg mL^{-1}). 1.25 mL of NaOH (1 mol L^{-1}) was added to 1.25 mL of the MPA solution (4 mol L^{-1}). The reaction was allowed to proceed in a dark room at 4 °C for 1 hour. The reaction mixture was purified by dialyzing it in a 3500 KD dialysis bag, first in a phosphate buffer solution (pH = 3, 20 mmol L^{-1}) for 24 hours and then in deionized water for another 24 hours. The resulting solution was stored at 4 °C under dark conditions.[61]

Detection procedures

To construct the REEI sensor array detection platform, 200 μL of each REEI (Sc^{3+}, Gd^{3+}, Lu^{3+}, Y^{3+}, Ce^{3+}, Pr^{3+}, Yb^{3+}, Dy^{3+}, Tm^{3+}, Sm^{3+}, Ho^{3+}, Tb^{3+}, La^{3+}, and Eu^{3+}) was mixed with 100 μL of ATT-AuNCs and BSA/MPA-AuNCs in a glycine–NaOH (Gly–NaOH) buffer (pH = 8.0, 50 mmol L^{-1}) to a total volume of 2 mL. The mixtures were allowed to react at room temperature for 5 minutes. The fluorescence intensity of the ATT-AuNC mixtures was measured at an excitation wavelength of 470 nm, and the fluorescence intensity of the BSA/MPA-AuNC mixtures was measured at 250 nm. Each REEI was tested in parallel five times, resulting in a training data matrix of 2 channels × 14 REEIs × 5 repetitions. The raw fluorescence data were processed using the formula $(F_0 - F)/F_0$, where F_0 is the fluorescence intensity of the probe without REEIs and F is the fluorescence intensity with REEIs. This normalization minimizes potential biases due to signal intensity differences. The processed data were analyzed using HCA and LDA in SPSS 25.0.
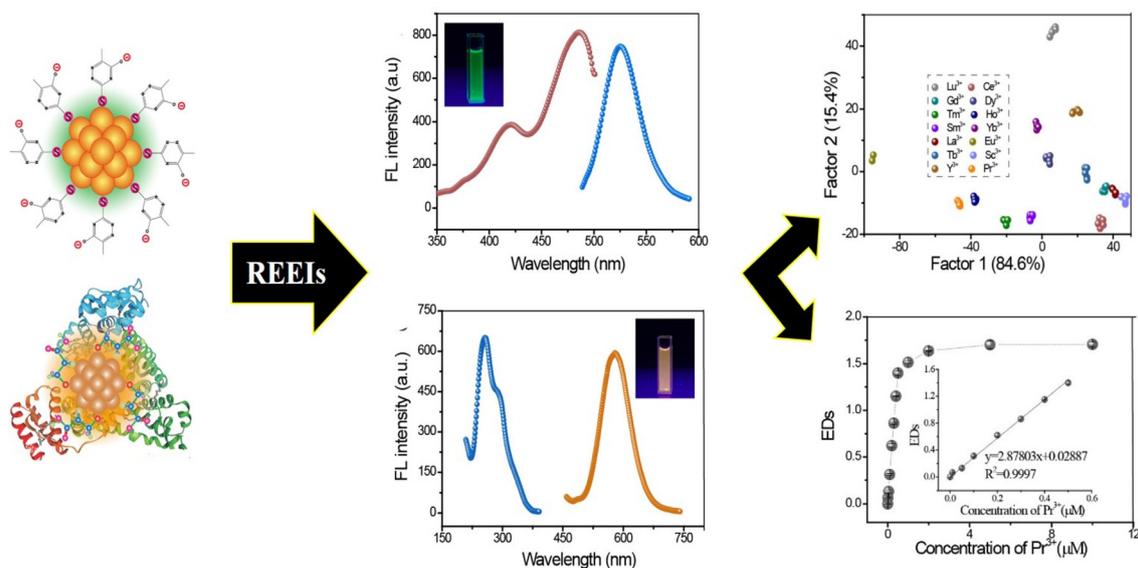
Scheme 1 Illustration of a fluorescence sensor array using ATT-AuNCs and BSA/MPA-AuNCs for detecting 14 rare earth element ions (REEIs).
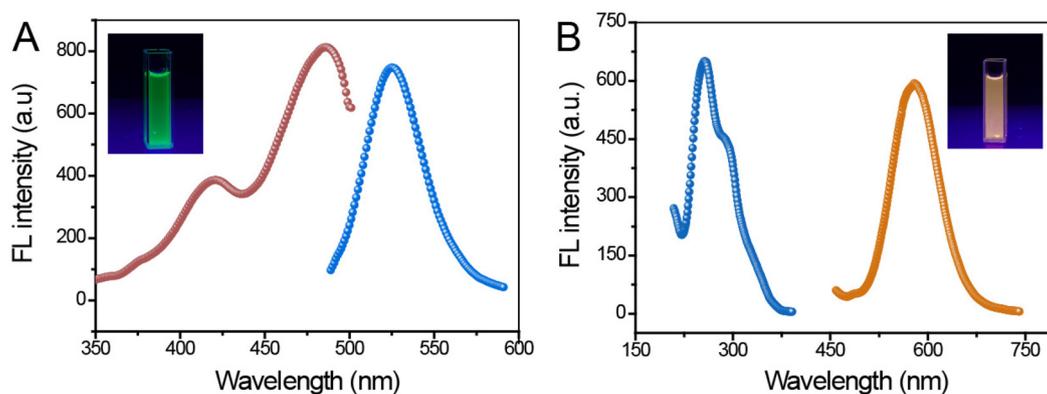
Fig. 1 (A) The red line represents the photoexcitation spectrum and the blue line indicates the photoemission spectrum of ATT-AuNCs. The inset displays a photograph of ATT-AuNCs illuminated with UV light. (B) The blue line shows the photoexcitation spectrum and the yellow line represents the photoemission spectrum of BSA/MPA-AuNCs. The inset includes a photograph of BSA/MPA-AuNCs under UV light.

Fluorescence response graphs were created using Origin 8.5 to evaluate the response capabilities of ATT-AuNCs and BSA/MPA-AuNCs to different REEIs.

Results and discussion

Synthesis and characterization of the sensor array of materials

Our previous research demonstrated that the presence of REEIs results in either quenching or enhancing the emission of AuNCs.[57,58] Consequently, we developed a sensor array utilizing two AuNC-based probes (*i.e.*, ATT-AuNCs and BSA/MPA-AuNCs) for the qualitative and quantitative analysis of various REEIs based on the distinct fluorescence spectra generated by the interactions between the probes and individual REEI. The preparation of these two fluorescent probes was

carried out as previously described.[60,61] Fig. 1 illustrates that the excitation wavelengths of ATT-AuNCs and BSA/MPA-AuNCs are 470 nm (with an emission wavelength of 520 nm) and 250 nm (with an emission wavelength of 580 nm), respectively. These results are consistent with spectra from our prior studies.[60,61] The left and right insets display the green fluorescence of ATT-AuNCs and the orange fluorescence of BSA/MPA-AuNCs under UV light, respectively. These results confirm the successful synthesis of the two fluorescent probes.

Feasibility of the constructed sensor array platform for REEI detection

To establish a sensor array detection platform for REEIs, we utilized ATT-AuNCs and BSA/MPA-AuNCs to detect 14 REEIs at a concentration level of 2 μmol L^{-1}. As depicted in Fig. 2A, the 14 REEIs exhibited distinct responses to both ATT-AuNCs and
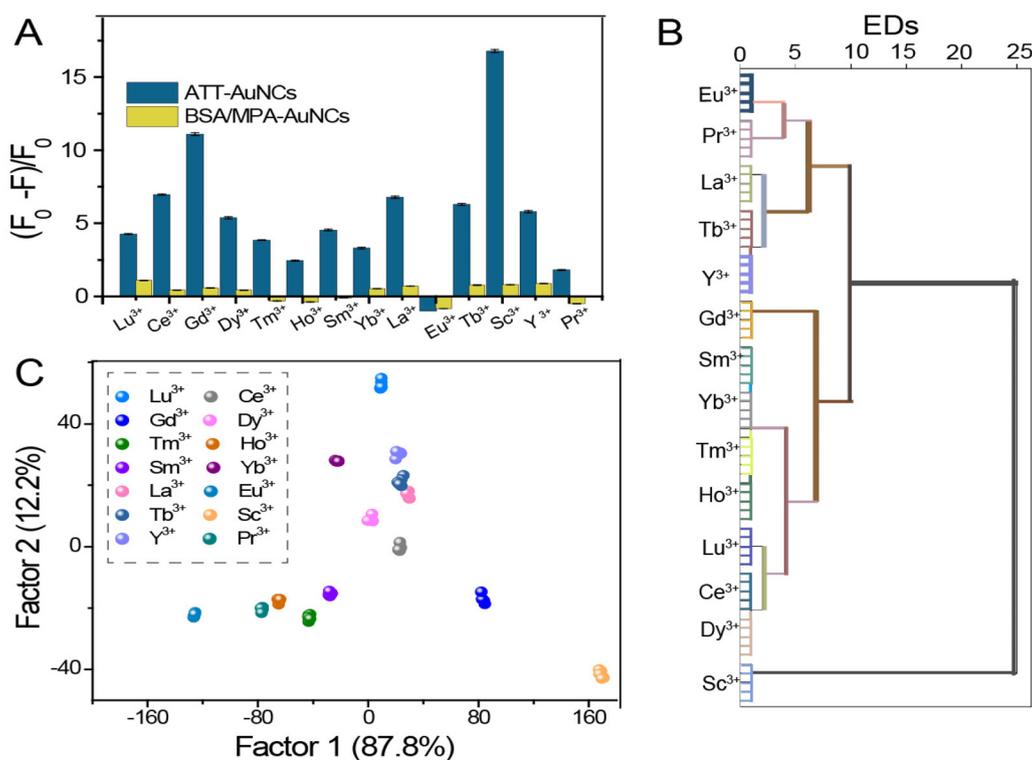
Fig. 2 (A) Histogram showing the response capabilities of the ATT-AuNC and BSA/MPA-AuNC probes to 14 REEIs. (B) Dendrogram generated using HCA. (C) Cluster diagram obtained through LDA. The final concentration of all REEIs was 2 µmol L^{-1}.

BSA/MPA-AuNCs, generating diverse signal inputs based on their respective responses. Upon closer examination of this figure, it is evident that Eu^{3+} induces a quenching effect on the fluorescence of both probes, while other elements have only minor impacts in the case of BSA/MPA-AuNCs, likely due to the PET effect.[57] Conversely, the other REEIs have noticeable enhancement effects on ATT-AuNCs, which may be attributed to the restriction of intramolecular motion (RIM) strategy.[58] Hierarchical cluster analysis (HCA) was employed to process the obtained data, resulting in the dendrogram shown in Fig. 2B, where five sets of parallel experiments were well-clustered, with each REEI forming distinct clusters, indicating clear differentiation among the 14 REEIs without interference. Subsequently, the differential signals were subjected to linear discriminant analysis (LDA), yielding the discriminant plot depicted in Fig. 2C, which achieved a discrimination accuracy of 100%. From Fig. 2C, it can be observed that the signals from multiple parallel experiments were stable, forming distinct clusters without overlap or interference between groups. The results from both HCA and LDA demonstrated the feasibility of the proposed method utilizing a double-probe sensor array for detecting the 14 REEIs. Consequently, it is highly recommended to utilize the proposed sensor array for detecting REEIs at various concentrations to ensure its validity.

To further evaluate the detection performance of this strategy, we expanded the concentration range of REEIs and tested concentrations of 0.5 µmol L^{-1} and 1 µmol L^{-1}. The LDA algor-

ithm was applied to generate the cluster plots shown in Fig. 3A and B. From Fig. 3, it is evident that the majority of cluster points are distributed independently and can be directly distinguished. While a small portion of the area may not be directly distinguishable due to the size of the viewing sphere, the detection accuracy in those regions remained at 100%. This suggests that our proposed detection platform using ATT-AuNCs and BSA/MPA-AuNCs demonstrates outstanding performance in identifying the selected REEIs across various concentrations. These findings encourage us to utilize our method for the quantitative analysis of the selected REEIs.

Quantitative analysis of the selected REEIs

Due to their significant impact on health and the environment, performing the quantitative analysis of REEIs is crucial. To assess the quantitative detection capability of the sensor for REEIs, we selected four specific ions, namely Dy^{3+}, Sc^{3+}, Lu^{3+}, and Pr^{3+} as evaluation standards, establishing a series of gradient concentrations for quantitative assessment. Standard curves were plotted for various REEIs present in the system. As depicted in Fig. 4A1, the sensor exhibited distinct responses to different concentrations of Dy^{3+}, with a gradual rise followed by a decline in trends. Processing via LDA computation, the clustered points in Fig. 4B1 demonstrated a consistent response trend similar to that in Fig. 4A1, achieving a 100% accuracy rate. Plotting each concentration point and utilizing
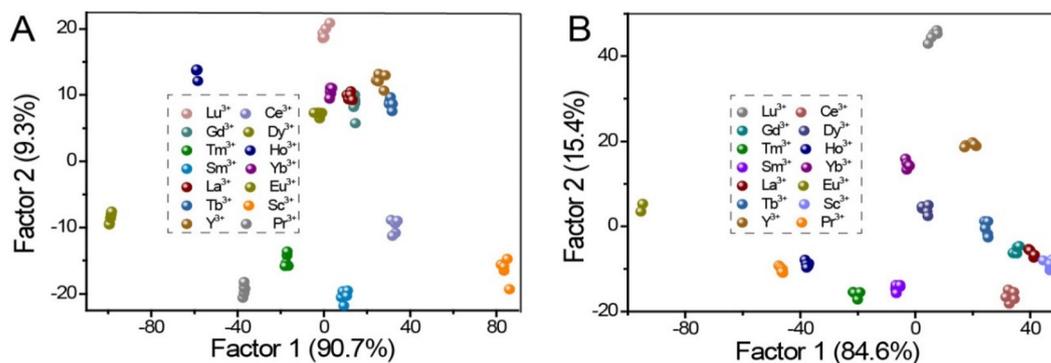
Fig. 3 Canonical score plots for the sensing array using the ATT-AuNC and BSA/MPA-AuNC probes to differentiate 14 REEIs at (A) 0.5 μmol L^{-1} and (B) 1 μmol L^{-1}.
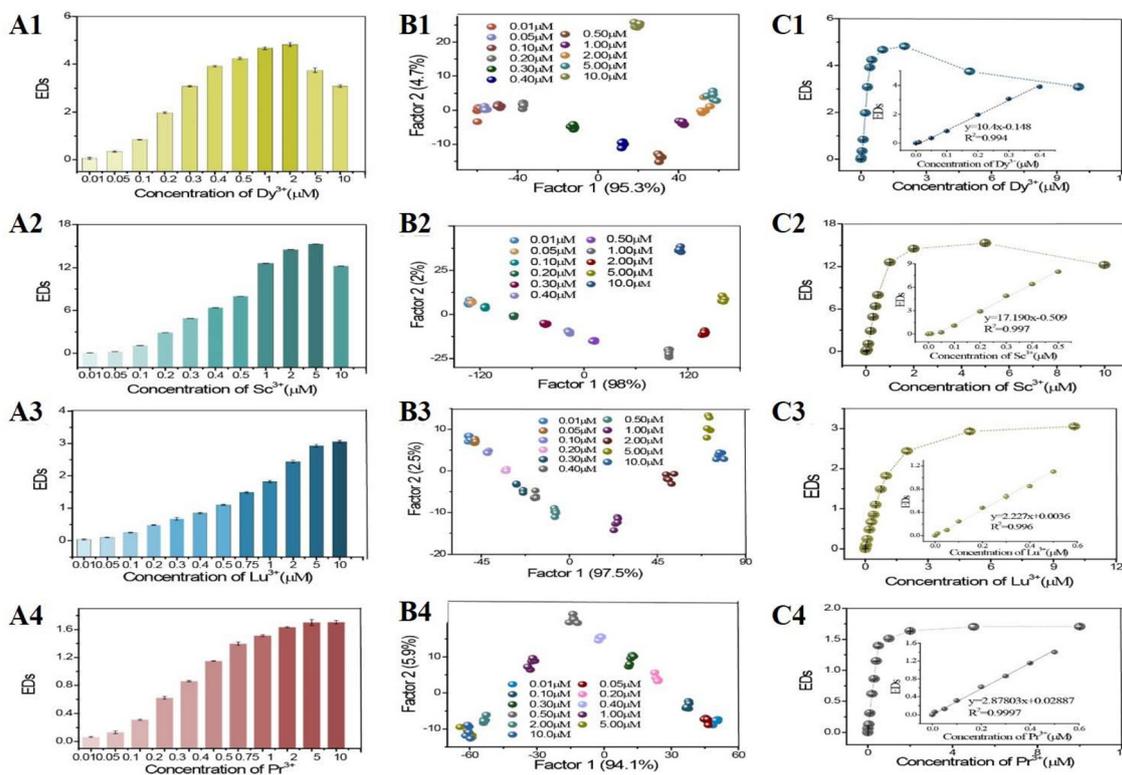

Fig. 4 (A1–4) Histograms showing the response capabilities of ATT-AuNCs and BSA/MPA-AuNCs at various concentrations of REEIs. (B1–4) Cluster diagrams generated using LDA. (C1–4) ED diagrams for the sensing array based on different concentrations of REEIs. The insets depict the linear relationship between EDs and the concentrations of REEIs.

the Euclidean Distance (ED) as the vertical axis,[21] Fig. 4C1 shows a linear relationship within the 0.05–0.4 μmol L^{-1} concentration range, with an R^2 value of 0.994 and a low detection limit (LOD) of 7.3 nmol L^{-1} (LOD = $3\sigma/S$, where σ represents the standard deviation of the blank response (or noise) and S is the slope of the calibration curve). Similarly, for Sc^{3+}, Lu^{3+}, and Pr^{3+} (Fig. 4A2–4, B2–4, and C2–4, respectively), LDA computations yielded a 100% accuracy rate, with a linear range of 0.05–0.5 μmol L^{-1} and R^2 values of 0.997, 0.996, and 0.999, respectively. LOD values were determined to be 0.2 nmol L^{-1} for Sc^{3+}, 14.3 nmol L^{-1} for Pr^{3+}, and 15.8 nmol L^{-1} for Dy^{3+}.

These findings underscore the suitability of this strategy not only for the identification but also for the quantitative detection of REEIs (Table 1).

Table 1 LOD values of the selected 4 REEIs

Rare earth ion	Linear range (μmol L^{-1})	LOD (nmol L^{-1})
Dy^{3+}	0.05–0.5	7.3
Sc^{3+}	0.05–0.5	0.2
Lu^{3+}	0.05–0.5	14.3
Pr^{3+}	0.05–0.5	15.8

Detection of REEIs at different ratios

To validate the sensor's detection performance for mixed samples, two REEIs (Lu^{3+} and Pr^{3+}) were chosen for mixing in different ratios at a total concentration of 1 µmol L^{-1} (*i.e.*, $Lu^{3+}:Pr^{3+}$ = 9:1, 8:2, 7:3, 6:4, 5:5, 4:6, 3:7, 2:8, and 1:9). As observed in Fig. 5A, the fluorescence rates of both probes showed an increasing trend as the proportion of Lu^{3+} decreased and Pr^{3+} increased. From Fig. 2A, it is evident that Lu^{3+} has a greater impact on both probes compared to Pr^{3+} (Fig. 5A). Furthermore, the data were processed *via* LDA, resulting in a 100% accuracy rate. The clustered points in Fig. 5B were independently distributed and non-overlapping, indicating the double-probe detection strategy's effectiveness in distinguishing mixed REEI samples. This result suggests that the proposed fluorescent sensing array has a high capability for differentiating between mixtures of REEIs. Altogether, these results demonstrate that the proposed sensor array has potential for the qualitative and quantitative detection of REEIs, suggesting the feasibility of applying this approach to detect REEIs in real-world samples.

The selectivity and applicability of the proposed sensor array

We selected a range of common metal ions (Na^+, K^+, Ca^{2+}, Zn^{2+}, Mg^{2+}, Fe^{3+}, Cu^{2+}, and Ba^{2+}) to test the selectivity and interference resistance of our sensor array, thereby validating the reliability of the sensor strategy designed. As depicted in Fig. 6A, the black clustered points represent interfering metal ions, while the rest represent the 14 REEIs. The interfering metal ions and the detected REEIs are mutually independent, allowing for good differentiation. These results confirm the high selectivity of our proposed sensor array for detecting the selected REEIs, indicating its potential suitability for real-world applications.

Additionally, by testing commercially available purified water from a certain brand to assess whether it contains REEIs and complies with food quality safety, we prepared a glycine–NaOH buffer detection system with pH = 8, added REEIs at a concentration of 1 µmol L^{-1}, and processed the obtained data using LDA to produce the cluster plot. From Fig. 6B, it is evident that all the selected REEIs form individual clusters and are independently distributed, with no overlapping or interference between the clusters. The accuracy of the results was 100%, indicating that the sensing detection platform con-
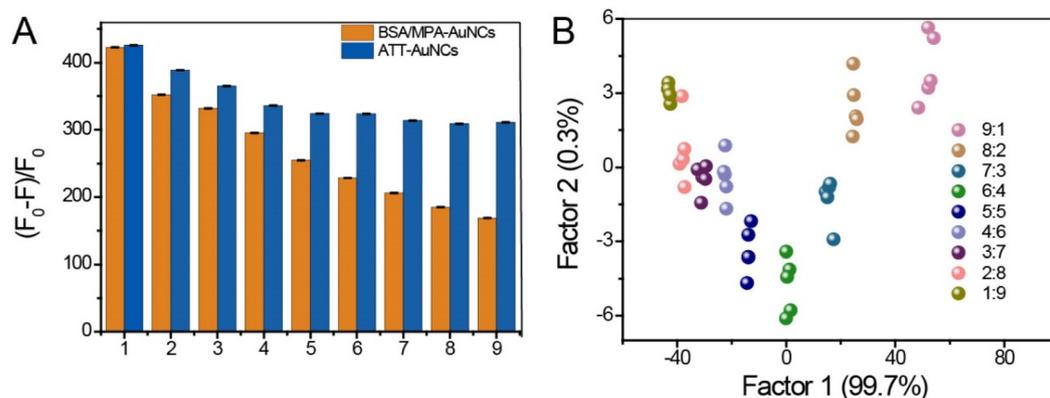

Fig. 5 (A) Histogram displaying the response of the probes at varying ratios of Lu^{3+} and Pr^{3+} at a total concentration of 1 µM, with ratios ranging from 9:1 to 1:9 for Lu^{3+} to Pr^{3+}, respectively. (B) Cluster diagram of the mixed sample as calculated using LDA.
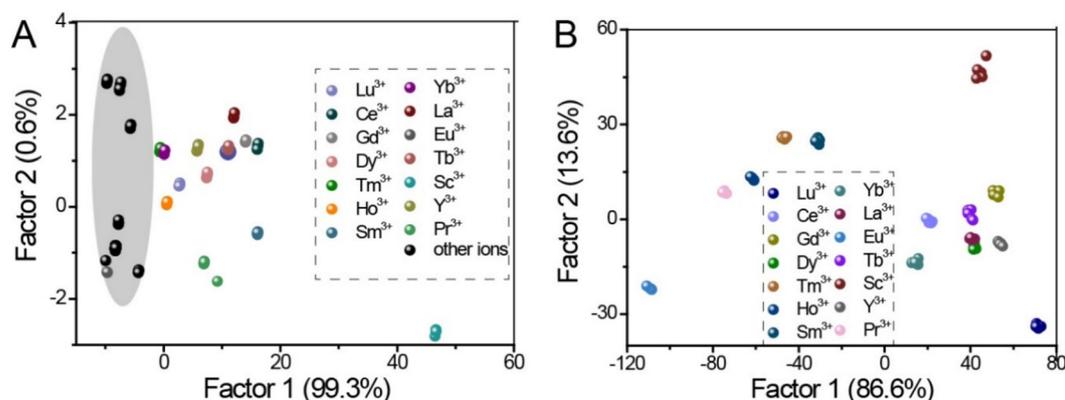

Fig. 6 (A) Cluster diagram illustrating the impact of common metal ions and 14 REEIs on the double probe. (B) Cluster diagram depicting the response of the double probe to 14 REEIs in real-world samples.

structed in this study can detect REEIs in actual samples and has significant potential for qualitative and quantitative analysis in complex testing environments. Therefore, this approach could be effectively utilized as a sensitive, selective, rapid, and reliable biosensor for monitoring various REEIs in the biomedical, environmental, and food industry sectors.

Conclusion

In summary, this study utilized ATT-AuNCs and BSA/MPA-AuNCs to detect 14 REEIs, establishing a simple, sensitive, and multi-target analysis fluorescent sensor array detection platform. We observed that REEIs have varying enhancement or quenching effects on ATT-AuNCs and BSA/MPA-AuNCs. Consequently, we considered these two probes as distinct signal channels and used the different effects of REEIs as signal inputs. Utilizing the cross-response phenomena of REEIs with ATT-AuNCs and BSA/MPA-AuNCs, we employed pattern recognition methods (*i.e.*, HCA and LDA) to create a "fingerprint map" of the targets, enabling discrimination and differentiation of various REEIs. By leveraging these pattern recognition techniques, we achieved excellent differentiation of REEIs, with a classification accuracy of 100%. Besides the outstanding identification capability for individual REEIs, this platform is also capable of distinguishing mixed REEIs. Through testing commercially available purified water containing doped REEIs, we further validated the practical application of the sensor array, with a classification accuracy of 100%. As the fluorescent sensor array comprises only two probes, this strategy reduces the synthesis and optimization of new probes, thus potentially aiding in the simple and effective identification of multiple REEIs. This study provides a new method for the simultaneous determination and identification of various analytes, filling the gap in REEI-based sensor array detection.

Author contributions

Hamada A. A. Noreldeen conceived the study and drafted the initial manuscript. Chen-Ting Zhu contributed to the method development and conducted the investigation. Kai-Yuan Huang, Hua-Ping Peng, and Hao-Hua Deng were involved in the manuscript review and editing. Wei Chen offered guidance, contributed to the study's conceptualization, and reviewed and edited the manuscript.

Data availability

The data will be available upon reasonable request.

Conflicts of interest

The authors state that they have no apparent competing financial interests or personal relationships that could have influenced the work presented in this paper.

References

1 M. Adeel, J. Y. Lee, M. Zain, M. Rizwan, A. Nawab, M. A. Ahmad, M. Shafiq, H. Yi, G. Jilani, R. Javed, R. Horton, Y. Rui, D. C. W. Tsang and B. Xing, *Environ. Int.*, 2019, **127**, 785–800.

2 X. Huang, S. Han, W. Huang and X. Liu, *Chem. Soc. Rev.*, 2013, **42**, 173–201.

3 W. Zhan, Y. Guo, X. Gong, Y. Guo, Y. Wang and G. Lu, *Chin. J. Catal.*, 2014, **35**, 1238–1250.

4 K. Inagaki and H. Haraguchi, *Analyst*, 2000, **125**, 191–196.

5 M. Salas and B. Tuchweber, *Arch. Toxicol.*, 1976, **35**, 115–125.

6 E. E. Lachine, A. A. Noujaim, C. Ediss and L. I. Wieber, *Int. J. Appl. Radiat.*, 1976, **27**, 373–377.

7 C. Turra, *Int. J. Environ. Health Res.*, 2018, **28**, 23–42.

8 V. M. Lu, K. L. McDonald and H. E. Townley, *Nanomedicine*, 2017, **12**, 2389–2401.

9 A. Pałasz and P. Czekaj, *Acta Biochim. Pol.*, 2000, **47**, 1107–1114.

10 J. T. Neary, R. Laskey, C. van Breemen, J. Blicharska, L. O. B. Norenberg and M. D. Norenberg, *Brain Res.*, 1991, **566**, 89–94.

11 J. T. Neary, L. O. B. Norenberg and M. D. Norenberg, *J. Neurochem.*, 1988, **50**, 1179–1184.

12 J. T. Neary, C. van Breemen, E. Forster, L. O. B. Norenberg and M. D. Norenberg, *Biochem. Biophys. Res. Commun.*, 1988, **157**, 1410–1416.

13 P. Peng, N. Wu, L. Ye, F. Jiang, W. Feng, F. Li, Y. Liu and M. Hong, *ACS Nano*, 2020, **14**, 16672–16680.

14 Y. Gu, Z. Guo, W. Yuan, M. Kong, Y. Liu, Y. Liu, Y. Gao, W. Feng, F. Wang, J. Zhou, D. Jin and F. Li, *Nat. Photonics*, 2019, **13**, 525–531.

15 H. Zou, L. Wang, C. Zeng, X. Gao, Q. Wang and S. Zhong, *Front. Mater. Sci.*, 2018, **12**, 327–347.

16 L. M. Aguirre-Díaz, N. Snejko, M. Iglesias, F. Sánchez, E. Gutiérrez-Puebla and M. Monge, *Inorg. Chem.*, 2018, **57**, 6883–6892.

17 B. Wang and B. Yan, *Talanta*, 2020, **208**, 120438.

18 V. K. Jain, A. Handa, S. S. Sait, P. Shrivastav and Y. K. Agrawal, *Anal. Chim. Acta*, 2001, **429**, 237–246.

19 A. N. Masi and R. A. Olsina, *Talanta*, 1993, **40**, 931–934.

20 M. Ayranov, J. Cobos, K. Popa and V. V. Rondinella, *J. Rare Earths*, 2009, **27**, 123–127.

21 H. A. A. Noreldeen, L. Yang, X. Y. Guo, S. B. He, H. P. Peng, H. H. Deng and W. Chen, *Analyst*, 2021, **147**, 101–108.

22 A. A. Essawy, *Sens. Actuators, B*, 2014, **196**, 640–646.

23 T. Terai, K. Kikuchi, S.-y. Iwasawa, T. Kawabe, Y. Hirata, Y. Urano and T. Nagano, *J. Am. Chem. Soc.*, 2006, **128**, 8699–8700.

24 Z. Li, S. Zhang, T. Yu, Z. Dai and Q. Wei, *Anal. Chem.*, 2019, **91**, 10448–10457.

25 F. Najafzadeh, F. Ghasemi and M. R. Hormozi-Nezhad, *Sens. Actuators, B*, 2018, **270**, 545–551.

26 W. Liu, F. Ding, Y. Wang, L. Mao, R. Liang, P. Zou, X. Wang, Q. Zhao and H. Rao, *Sens. Actuators, B*, 2018, **265**, 310–317.

27 H. A. A. Noreldeen, K.-Y. Huang, G.-W. Wu, H.-P. Peng, H.-H. Deng and W. Chen, *Anal. Chem.*, 2022, **94**, 9287–9296.

28 H. A. A. Noreldeen, K.-Y. Huang, G.-W. Wu, Q. Zhang, H.-P. Peng, H.-H. Deng and W. Chen, *Anal. Chem.*, 2022, **94**, 17533–17540.

29 C.-T. Zhu, K.-Y. Huang, Q.-L. Zhou, X.-P. Zhang, G.-W. Wu, H.-P. Peng, H.-H. Deng, W. Chen and H. A. A. Noreldeen, *Spectrochim. Acta, Part A*, 2023, **288**, 122138.

30 H. A. A. Noreldeen, S.-B. He, K.-Y. Huang, C.-T. Zhu, Q.-L. Zhou, H.-P. Peng, H.-H. Deng and W. Chen, *Anal. Bioanal. Chem.*, 2022, **414**, 8365–8378.

31 J. Sun, Y. Lu, L. He, J. Pang, F. Yang and Y. Liu, *TrAC, Trends Anal. Chem.*, 2020, **122**, 115754.

32 Y. Ma, Y. Li, K. Ma and Z. Wang, *Sci. China: Chem.*, 2018, **61**, 643–655.

33 X. Li, S. Li, Q. Liu, Z. Cui and Z. Chen, *ACS Sustainable Chem. Eng.*, 2019, **7**, 17482–17490.

34 Z. Li and K. S. Suslick, *ACS Sens.*, 2018, **3**, 121–127.

35 S. Sun, K. Jiang, S. Qian, Y. Wang and H. Lin, *Anal. Chem.*, 2017, **89**, 5542–5548.

36 Y. Pei, P. Wang, Z. Ma and L. Xiong, *Acc. Chem. Res.*, 2019, **52**, 23–33.

37 C. Guo and J. Irudayaraj, *Anal. Chem.*, 2011, **83**, 2883–2889.

38 R. Liu, Y. Wang, Y. Cui, Z. Sun, Y. Wei and X. J. A. A. S. Gao, *Acta Agron. Sin.*, 2013, **40**, 977.

39 L. Shang, S. Dong and G. U. Nienhaus, *Nano Today*, 2011, **6**, 401–418.

40 L.-Y. Chen, C.-W. Wang, Z. Yuan and H.-T. Chang, *Anal. Chem.*, 2015, **87**, 216–229.

41 Y. Zheng, L. Lai, W. Liu, H. Jiang and X. Wang, *Adv. Colloid Interface Sci.*, 2017, **242**, 1–16.

42 H.-H. Deng, K.-Y. Huang, Q.-Q. Zhuang, Q.-Q. Zhuang, H.-P. Peng, Y.-H. Liu, X.-H. Xia and W. Chen, *Microchim. Acta*, 2018, **185**, 400.

43 A. Mathew and T. Pradeep, *Part. Part. Syst. Charact.*, 2014, **31**, 1017–1053.

44 X.-P. Zhang, K.-Y. Huang, S.-B. He, H.-P. Peng, X.-H. Xia, W. Chen and H.-H. Deng, *J. Hazard. Mater.*, 2021, **405**, 124259.

45 N. Cao, J. Xu, H. Zhou, Y. Zhao, J. Xu, J. Li and S. Zhang, *Microchem. J.*, 2020, **159**, 105406.

46 Y. Gui, Y. Wang, C. He, Z. Tan, L. Gao, W. Li and H. Bi, *J. Mater. Chem. C*, 2021, **9**, 2833–2839.

47 D. Bain, S. Maity, B. Paramanik and A. Patra, *ACS Sustainable Chem. Eng.*, 2018, **6**, 2334–2343.

48 X. Wei, Z. Chen, L. Tan, T. Lou and Y. Zhao, *Anal. Chem.*, 2017, **89**, 556–559.

49 X. Han, Z. Man, S. Xu, L. Cong, Y. Wang, X. Wang, Y. Du, Q. Zhang, S. Tang, Z. Liu and W. Li, *Colloids Surf., B*, 2019, **173**, 478–485.

50 Y. Wu, B. Wang, K. Wang and P. Yan, *Anal. Methods*, 2018, **10**, 3939–3944.

51 S. Xu, X. Lu, C. Yao, F. Huang, H. Jiang, W. Hua, N. Na, H. Liu and J. Ouyang, *Anal. Chem.*, 2014, **86**, 11634–11639.

52 W. Miao, L. Wang, Q. Liu, S. Guo, L. Zhao and J. Peng, *Chem. – Asian J.*, 2021, **16**, 247–251.

53 J. Peng, Y. Su, F.-Q. Huang, Q. Zuo, L. Yang, J. Li, L. Zhao and L.-W. Qi, *J. Colloid Sci.*, 2019, **539**, 175–183.

54 H. Yang, F. Lu, Y. Sun, Z. Yuan and C. Lu, *Anal. Chem.*, 2018, **90**, 12846–12853.

55 Z. Shojaeifard, M. M. Bordbar, M. D. Aseman, S. M. Nabavizadeh and B. Hemmateenejad, *Sens. Actuators, B*, 2021, **334**, 129582.

56 Y. Tao, M. Li and D. T. Auguste, *Biomaterials*, 2017, **116**, 21–33.

57 L.-F. Xiu, K.-Y. Huang, C.-T. Zhu, Q. Zhang, H.-P. Peng, X.-H. Xia, W. Chen and H.-H. Deng, *Langmuir*, 2021, **37**, 949–956.

58 K.-Y. Huang, L.-F. Xiu, X.-Y. Fang, M.-R. Yang, H. A. A. Noreldeen, W. Chen and H.-H. Deng, *J. Phys. Chem. Lett.*, 2022, **13**, 9526–9533.

59 Y. Yang, C. Wei, W. Wang, H. A. A. Noreldeen, Z. Huang, H. Deng, H. Peng, X. Xia and W. Chen, *ChemComm*, 2022, **58**, 6219–6222.

60 H.-H. Deng, X.-Q. Shi, F.-F. Wang, H.-P. Peng, A.-L. Liu, X.-H. Xia and W. Chen, *Chem. Mater.*, 2017, **29**, 1362–1369.

61 H.-H. Deng, F.-F. Wang, X.-Q. Shi, H.-P. Peng, A.-L. Liu, X.-H. Xia and W. Chen, *Biosens. Bioelectron.*, 2016, **83**, 1–8.